Stability Analysis of Simple Running Models

Ken

June, 2018*

1 Introduction

The purpose of this project is to analyze the stability (via Poincare map) of three simple running models to get a better understanding to the source of stability and robustness for fast runners. The three simple runners are:

- 2 DOF (Vertical) Hopper with pitch angle control
- Spring Loaded Inverted Pendulum (SLIP) model
- SLIP with Pendulum Runner (SLIPPER)

1.1 About the systems

In this analysis, all the models are 2D runners. The following are important common assumptions applied to all simple running models in this project

- The (steady-state) running motion is periodic.
- Massless leg – No impact will be induced during foot collision.
- Energy conservation (especially for passive runners)
- Open-loop control on leg (e.g. open-loop leg force, or fixed touch-down angle for SLIP-based runners)
- Closed-loop control on pitch angle

Important parameters or quantities

- Spring stiffness
- Running speed/running period/running frequency
- Duty factor = $\frac{t_{stance}}{t_{stance}+t_{flight}}$
- Fast running index (proposed by IHMC)

Other important concepts (of fast runner)

- Meta center
- Resonance – Please check Jorge Cham's thesis [11] 2.2 Resonance in Running.
- Please refer to fast runner meeting notes or proposal for more information.

*Last update: August 23, 2018

1.2 Related research

- Jorge Cham's Dissertation [11]
- David Remy's Dissertation [41]
- Shen's paper about SLIP model analysis [43]

1.3 About the method of stability analysis used in this project

Some "must-have" and "nice-to-have" requirements for the analysis method

- Stability analysis
- Robustness
- Dimension analysis (so that it can be used for robots with different scales)
- Applicable to complex system (e.g. for the designed mechanism)

For the requirements listed above, and also to explore the nonlinearity and coupled dynamics for SLIP-based runners, the main method for stability analysis used in this project contains two parts:

- Trajectory optimization using single-shooting method – For finding periodic motions.
- Poincare Map – Check the Eigen values of the Poincare map (it is a matrix) of a periodic motion to determine its stability.

Please refer to Description of how to find limit cycles and Poincare maps from Andy Ruina, the note has great numerical recipe for better Poincare map approximation and stability analysis.

1.3.1 About the Poincare section and Poincare map

Please check Jorge Cham's thesis [11] Chapter 2 for more information.

1.3.2 About the Trajectory optimization using single shooting method

This method is widely used for finding stable limit cycles for passive walkers. For more imformation, please check Matthew Kelly's web page about Canon examples using different trajectory optimization methods.

1.4 Fast running index

Please refer to fast runner meeting notes or proposal for more information.

1.5 Other links

- Ken's slides on the Confluence page
- project Repo: https://stash.ihmc.us/projects/ICSL/repos/fast-runner-analysis
- SCS implementation: RoundRunner under Fast Runner: https://stash.ihmc.us/projects/ICSL/repos/fast-runner/browse/fast-runner/src/main/java/us/ihmc/fastRunner/RoundRunner

2 Pitch Stability of an Vertically Open-loop Hopper

2.1 Jorge Cham's Dissertation - openloop control of 1DOF vertical hopper

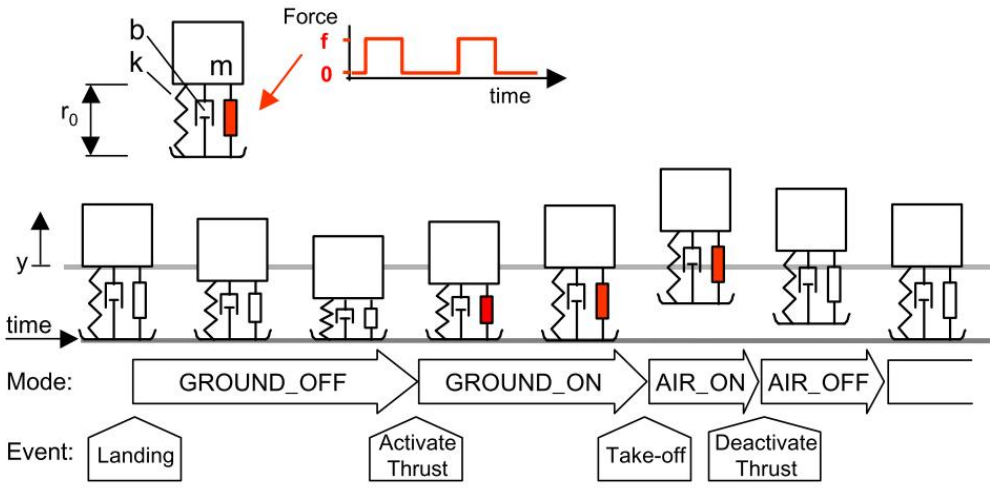

Figure 3-1. The vertical hopping model used for analysis. The hopper's leg consists of a spring, a damper and a force element which is active according to a binary motor pattern. The figure shows a sample trajectory of the hopper, the different modes that it goes through, and the events that trigger the transitions between the modes.

Figure 1: The schematic of a 1 DOF hopper [11]

2.1.1 Equation of motion

Using the model as shown in Fig. 1, during the stand phase (i.e. $y \leq 0$), the equation of motion can be expressed as:

$$m\ddot{y} = -b\dot{y} + -ky - mg + f$$

where m is the mass, b is the damping, k is the stiffness, f is the control input. Normalized by weight, the equation becomes

$$\ddot{y} = -b/m\dot{y} + -k/my - g + f/m$$

Expressed in state space form:

$$\begin{bmatrix}\dot{y}\\ \ddot{y}\end{bmatrix} = \begin{bmatrix}0 & 1\\ -k/m & -b/m\end{bmatrix}\begin{bmatrix}y\\ \dot{y}\end{bmatrix} + \begin{bmatrix}0\\ -g + f/m\end{bmatrix} \tag{1}$$

or equivalently

$$\dot{X} = \begin{bmatrix}0 & 1\\ -\omega^2 & -2\xi\omega\end{bmatrix}X + \begin{bmatrix}0\\ -g + f_n(t)\end{bmatrix} = \begin{bmatrix}0 & 1\\ -k_p & -k_d\end{bmatrix}X + \begin{bmatrix}0\\ -g + f_n(t)\end{bmatrix} \tag{2}$$

where $X \triangleq [y, \dot{y}]^T$. When the hopper is in the air (i.e. $y > 0$, flight phase),

$$\dot{X} = \begin{bmatrix}0 & 1\\ 0 & 0\end{bmatrix}X + \begin{bmatrix}0\\ -g\end{bmatrix} \tag{3}$$

Define the force of an open-loop motor pattern

$$f_n(t) = \begin{cases} f/m, & \text{if } t_{off} < t < t_{off} + t_{on}. \\ 0, & \text{otherwise.} \end{cases} \tag{4}$$

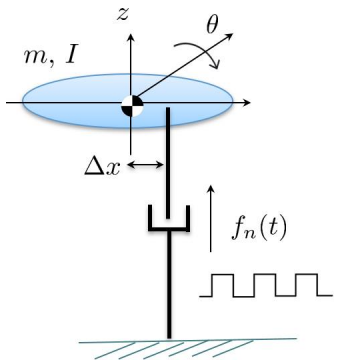

Figure 2: The schematic of a 2 DOF hopper

2.2 Stability Analysis of an Open-loop Controlled Hopper with Discrete Pitch Angle Control

Use the state space of z motion form 2 with a simplified open-loop force input:

$$\begin{bmatrix} \dot{z} \\ \ddot{z} \end{bmatrix} = \begin{bmatrix} 0 & 1 \\ -kp_z & -kd_z \end{bmatrix} \begin{bmatrix} z \\ \dot{z} \end{bmatrix} + \begin{bmatrix} 0 \\ -g + f_n(t) \end{bmatrix} \tag{5}$$

where

$$f_n(t) = \begin{cases} f_n \triangleq f/m, & \text{if } t_{flight} < t < t_{flight} + t_{contact}. \\ 0, & \text{otherwise.} \end{cases} \tag{6}$$

To further simplify the problem, assuming $f_n(t)$ is much more dominant than $-kp_z z - kd_z \dot{z}$-g so that:

$$\begin{bmatrix} \dot{z} \\ \ddot{z} \end{bmatrix} \approx \begin{bmatrix} 0 & 1 \\ 0 & 0 \end{bmatrix} \begin{bmatrix} z \\ \dot{z} \end{bmatrix} + \begin{bmatrix} 0 \\ f_n(t) \end{bmatrix} \tag{7}$$

Assumptions:

- $f_n(t)$[1] can induce stable vertical hopping motion.
- t_0 starts when the foot leaves the ground.
- $t_{flight} + t_{contact} = T$, $t_{contact} = \alpha$, and $T > \alpha$

Then for the 2 DOF vertical hopper as shown in Fig. 2, the pitch dynamics with feedback control can be expressed as:

$$\begin{bmatrix} \dot{\theta} \\ \ddot{\theta} \end{bmatrix} = \begin{bmatrix} 0 & 1 \\ 0 & 0 \end{bmatrix} \begin{bmatrix} \theta \\ \dot{\theta} \end{bmatrix} + \begin{bmatrix} 0 \\ -f_n(t) m / I \Delta x \end{bmatrix} \tag{8}$$

[1]Conceptually, the $f_n(t)$ can be treated as a force applied from a nonlinear component which connects the massless leg to the body (so there is no velocity change happen at foot strike)

2.2.1 Poincare Section

Denote the state at the n^{th} step Poincare section $\theta_n, \dot{\theta}_n$ (defined at the start of the flight phase). Then we can calculate the state at Poincare section at the $n+1^{th}$ step:

$$\dot{\theta}_{n+1} = \dot{\theta}_n - \frac{f}{I}\Delta x t_{contact} \tag{9}$$

$$\theta_{n_{touchDown}} = \theta_n + \dot{\theta}_n t_{flight}$$

$$\dot{\theta}_{n_{touchDown}} = \dot{\theta}_n$$

$$\begin{aligned}\theta_{n+1} &= \theta_n + \dot{\theta}_n t_{flight} + \dot{\theta}_n t_{contact} - \frac{1}{2}\frac{f}{I}\Delta x t_{contact}^2 \\ &= \theta_n + T\dot{\theta}_n - \frac{1}{2}\frac{f}{I}\alpha^2 \Delta x\end{aligned} \tag{10}$$

2.2.2 Poincare Map of Pitch Dynamics with Proportional Control

By designing a proportional control such that $\Delta x = k\phi_n$ and defining $K = \frac{1}{2}\frac{f}{I}k$, Eq. 9 and Eq.10 can be expressed as follows:

$$\begin{aligned}\theta_{n+1} &= \theta_n - \alpha^2 K\theta_n + T\dot{\theta}_n \\ \dot{\theta}_{n+1} &= \dot{\theta}_n - 2\alpha K\theta_n\end{aligned}$$

Arranged them in the state space equation, we can get a discrete map M (i.e. Poincare Map, with set of difference equations):

$$\begin{bmatrix}\theta_{n+1} \\ \dot{\theta}_{n+1}\end{bmatrix} = \begin{bmatrix}1-\alpha^2 K & T \\ -2\alpha K & 1\end{bmatrix}\begin{bmatrix}\theta_n \\ \dot{\theta}_n\end{bmatrix} = M\begin{bmatrix}\theta_n \\ \dot{\theta}_n\end{bmatrix} \tag{11}$$

Eigen value analysis
To analyze the stability of the equation in 11, we need to check whether the eigen values of Poincare map M are within the unit cycle. Similar to the Rooth-Herwitz method for the continuous map, we can use Jury Stability Test (Ogata, 1985)[2], which states that a discrete system of two dimensions with the characteristic equations P(z) of the form:

$$P(z) = a_0 z^2 + a_1 z + a_2$$

where $a_0 > 0$, is stable if the following conditions are all satisfied:

$$\begin{aligned}|a_2| &< a_0 \\ a_0 + a_1 + a_2 &> 0 \\ a_0 - a_1 + a_2 &> 0 \\ |(a_0 + a_2)(a_2 - a_0)| &> |a_1(a_0 - a_1)|\end{aligned}$$

For a Jacobian of the form

$$J = \begin{bmatrix}J_1 & J_2 \\ J_3 & J_4\end{bmatrix}$$

The characteristics equation can be expressed as follows:

$$P(z) = z^2 - (J_1 + J_4)z + (J_1 J_4 - J_2 J_3)$$

[2]contents quotated from [11]

Substituting into the stable conditions stated above,

$$|(J_1J_4 - J_2J_3)| < 1 \tag{12}$$
$$1 - (J_1 + J_4) + (J_1J_4 - J_2J_3) > 0 \tag{13}$$
$$1 + (J_1 + J_4) + (J_1J_4 - J_2J_3) > 0 \tag{14}$$
$$|(1 + (J_1J_4 - J_2J_3))((J_1J_4 - J_2J_3) - 1)| > |(J_1 + J_4)(1 + (J_1 + J_4)| \tag{15}$$

Check condition Eq.12:
First assuming $1 - \alpha^2K + 2T\alpha K > 0$

$$\begin{aligned} 1 - \alpha^2K + 2T\alpha K &< 1 \\ \rightarrow -\alpha^2K + 2T\alpha K &< 0 \\ \rightarrow \alpha K(-\alpha + 2T) &< 0 \end{aligned}$$

Since $\alpha > 0$, $K > 0$, and $T > \alpha$, the assumption cannot satisfy the condition.
Next, assuming $1 - \alpha^2K + 2T\alpha K < 0$:

$$\begin{aligned} 1 - \alpha^2K + 2T\alpha K &> -1 \\ \rightarrow -1 + \alpha^2K - 2T\alpha K &< 1 \\ \rightarrow \alpha K(\alpha - 2T) &< 2 \end{aligned}$$

Since $T > \alpha$, the condition can always be satisfied, as long as the following condition is satisfied:

$$(J_1J_4 - J_2J_3) = (1 - \alpha^2K + 2T\alpha K) < 0$$

Combine conditions above we can get a new inequality as follows:

$$-1 < (J_1J_4 - J_2J_3) = (1 - \alpha^2K + 2T\alpha K) < 0 \tag{16}$$

Check condition Eq.13:

$$\begin{aligned} 1 - (1 - \alpha^2K + 1) + (1 - \alpha^2K + 2T\alpha K) &> 0 \\ \rightarrow 2T\alpha K &> 0 \end{aligned}$$

From the last inequality we can get the condition is <u>always hold</u>.

Check condition Eq.14:

$$\begin{aligned} 1 + (1 - \alpha^2K + 1) + (1 - \alpha^2K + 2T\alpha K) &> 0 \\ \rightarrow 4 - 2\alpha^2K + 2T\alpha K &> 0 \\ \rightarrow 4 + \alpha K(-2\alpha + 2T) &> 0 \end{aligned}$$

From the last inequality we can get the condition is <u>always hold</u>.

Check condition Eq.15:
Based on Eq. 16, the left hand side of Eq. 15 can be rearranged as :

$$|(det(M) + 1)(det(M) - 1)| = |det(M)^2 - 1| = 1 - det(M)^2$$

From Eq. 13 and 14 we can got $(J_1 + J_4) > 0$, therefore the right hand side of Eq. 15 can be rearranged as:

$$|(J_1 + J_4)(J_1 + J_4 + 1)| = (J_1 + J_4)(J_1 + J_4 + 1)$$

Therefore the Eq. 15 can be expressed as follows:

$$1 - det(M)^2 > tr(M)(tr(M) + 1)$$

where $det(M) = \prod_i \lambda_i = (J_1 J_4 - J_2 J_3)$ is the determinant of matrix M and $tr(M) = \sum_i \lambda_i = (J_1 + J_4)$ is the trace of the matrix M.

To sum up
For the (Poincare) stability, the following conditions need to be satisfied:

$$-1 < det(M) < 0 \tag{17}$$

$$0 < tr(M)(tr(M) + 1) < 1 - det(M)^2 \tag{18}$$

where

$$\begin{aligned} det(M) &= 1 - \alpha^2 K + 2T\alpha K \\ tr(M) &= 2 - \alpha^2 K \\ K &= \frac{1}{2}\frac{f_n}{I}k \end{aligned}$$

Result
After check the sign of the $det(M)$, it was found that $det(M)$ always > 0:

$$1 - \alpha^2 K + 2T\alpha K = 1 + \alpha K(-\alpha + 2T) > 0$$

Therefore, it is concluded that proportional control with this system setup cannot stablize the pitch dynamics.

2.2.3 Poincare Map of Pitch Dynamics with PD Control

By designing a PD control such that $\Delta x = k_p\theta_n + k_d\dot{\theta}_n$ and defining $K = \frac{1}{2}\frac{f}{I}k_p$, $C = \frac{1}{2}\frac{f}{I}k_d$, Eq. 9 and Eq.10 can be expressed as follows:

$$\theta_{n+1} = \theta_n - \alpha^2 K\theta_n + T\dot{\theta}_n - \alpha^2 C\dot{\theta}_n$$
$$\dot{\theta}_{n+1} = \dot{\theta}_n - 2\alpha K\theta_n - 2\alpha C\dot{\theta}_n$$

Arranged them in the state space equation, we can get a discrete map M_{pd}:

$$\begin{bmatrix}\theta_{n+1}\\ \dot{\theta}_{n+1}\end{bmatrix} = \begin{bmatrix}1-\alpha^2 K & T-\alpha^2 C\\ -2\alpha K & 1-2\alpha C\end{bmatrix}\begin{bmatrix}\theta_n\\ \dot{\theta}_n\end{bmatrix} = M_{pd}\begin{bmatrix}\theta_n\\ \dot{\theta}_n\end{bmatrix} \tag{19}$$

2.2.4 Analytical Solution for Eq.7

Start from t_0 (the beginning of the flight phase), assuming $Z = [0, \dot{z}_0]^T$, then we can get:

$$z(t_{flight}) = \dot{z}_0 t_{flight} - 1/2 g t_{flight}^2 = 0 \tag{20}$$
$$\dot{z}(t_{flight}) = \dot{z}_0 - g t_{flight} = -\dot{z}_0 \tag{21}$$

where a constraint for the $\dot{z}_0$ can be derived:

$$\dot{z}_0 = 1/2 g t_{flight} \tag{22}$$
$$\tag{23}$$

Then we can derive the solution at the end of the touch down:

$$z(1) = -\dot{z}_0 t_{contact} + (f/m - g) t_{contact}^2 = 0 \tag{24}$$
$$\dot{z}(1) = -\dot{z}_0 + (f/m - g) t_{contact} = \dot{z}_0 \tag{25}$$

where another constraint for the $\dot{z}_0$ can be derived:

$$\dot{z}_0 = 1/2 (f/m - g) t_{contact} \tag{26}$$

Period T, contact force f and $t_{contact}$ are dependent From Eqs. 26 and 22 we can get

$$\begin{aligned} 1/2 g t_{flight} &= 1/2 (f/m - g) t_{contact} \\ \rightarrow t_{flight} &= (f/mg - 1) t_{contact} \\ \rightarrow t_{flight} + t_{contact} &= T = (f/mg) t_{contact} \end{aligned}$$

2.3 Stability Analysis of an Open-loop Controlled Hopper with Continuous Pitch Angle Control

Consider the case that $\Delta x = k\theta(t)$ or $\Delta x = k_p\theta(t) + k_d\dot{\theta}(t)$, then the pitch angle will be controlled continuously in the stance phase.

2.3.1 Poincare map of Hopper with Continuous Proportional Control

Assuming $\Delta x = k\theta(t)$, then the system dynamic in the stance phase becomes:

$$\dot{X} = \begin{bmatrix}\dot{\theta}\\ \ddot{\theta}\end{bmatrix} = \begin{bmatrix}0 & 1\\ -k\frac{f}{I} & 0\end{bmatrix} X \triangleq \begin{bmatrix}0 & 1\\ -2K & 0\end{bmatrix} X = AX \tag{27}$$

where $K = \frac{1}{2}\frac{f}{I}k$. Again denoting the state at the n^{th} step Poincare section $X_n = [\theta_n, \dot{\theta}_n]^T$ (defined at the start of the flight phase). Then we can first calculate the touchdown state at n_{th} step:

$$\begin{aligned}\theta_{n_{TD}} &= \theta_n + \dot{\theta}_n t_{flight}\\ \dot{\theta}_{n_{TD}} &= \dot{\theta}_n\end{aligned}$$

and $X_{n_{TD}} = [\theta_{n_{TD}}, \dot{\theta}_{n_{TD}}]^T$ then can be expressed as:

$$X_{n_{TD}} = \begin{bmatrix}1 & (T-\alpha)\\ 0 & 1\end{bmatrix} X_n \tag{28}$$

Next, assuming the contact time is exactly $t_{contact} = \alpha$ (e.g. no perturbation in z direction), then the $X_{n+1} = [\theta_{n+1}, \dot{\theta}_{n+1}]^T$ can be expressed with $X_{n_{TD}} = [\theta_{n_{TD}}, \dot{\theta}_{n_{TD}}]^T$:

$$X_{n+1} = e^{A\alpha}(X_{nTD} - X_{eq}) + X_{eq} \tag{29}$$

$$= e^{A\alpha}(\begin{bmatrix}1 & (T-\alpha)\\ 0 & 1\end{bmatrix} X_n - X_{eq}) + X_{eq} \tag{30}$$

where $X_{eq} = [0, 0]^T$ is the equilibrium point of Eq. 27. Therefore, we can get the Poincare map in this case is:

$$M = e^{A\alpha}(\begin{bmatrix}1 & (T-\alpha)\\ 0 & 1\end{bmatrix} \tag{31}$$

Using symbolic tool in MATLAB, we can derive the closed-form expression of M as follows:

$$M = \begin{bmatrix}M_{11} M_{12}\\ M_{21} M_{22}\end{bmatrix}$$

where

$$\begin{aligned}M_{11} =& \frac{\mathrm{e}^{\sqrt{2}\sqrt{-K}\,a}}{2} + \frac{\mathrm{e}^{-\sqrt{2}\sqrt{-K}\,a}}{2}\\ M_{12} =& \left(\frac{\mathrm{e}^{\sqrt{2}\sqrt{-K}\,a}}{2} + \frac{\mathrm{e}^{-\sqrt{2}\sqrt{-K}\,a}}{2}\right)(T-a) + \frac{\sqrt{2}\,\mathrm{e}^{\sqrt{2}\sqrt{-K}\,a} - \sqrt{2}\,\mathrm{e}^{-\sqrt{2}\sqrt{-K}\,a}}{4\sqrt{-K}}\\ M_{21} =& \frac{\sqrt{2}\sqrt{-K}\,\mathrm{e}^{\sqrt{2}\sqrt{-K}\,a}}{2} - \frac{\sqrt{2}\sqrt{-K}\,\mathrm{e}^{-\sqrt{2}\sqrt{-K}\,a}}{2}\\ M_{22} =& \frac{\mathrm{e}^{\sqrt{2}\sqrt{-K}\,a}}{2} + \frac{\mathrm{e}^{-\sqrt{2}\sqrt{-K}\,a}}{2} + \left(\frac{\sqrt{2}\sqrt{-K}\,\mathrm{e}^{\sqrt{2}\sqrt{-K}\,a}}{2} - \frac{\sqrt{2}\sqrt{-K}\,\mathrm{e}^{-\sqrt{2}\sqrt{-K}\,a}}{2}\right)(T-a)\end{aligned}$$

2.3.2 Poincare Map of Hopper with Continuous PD Control

Assuming $\Delta x = k_p\theta(t) + k_d\dot{\theta}(t)$, then the system dynamic in the stance phase becomes:

$$\dot{X} = \begin{bmatrix}\dot{\theta}\\ \ddot{\theta}\end{bmatrix} = \begin{bmatrix}0 & 1\\ -k_p\frac{f}{I} & -k_d\frac{f}{I}\end{bmatrix} X \triangleq \begin{bmatrix}0 & 1\\ -2K & -2C\end{bmatrix} X = AX \tag{32}$$

$$M_{pd} = e^{A\alpha}(\begin{bmatrix}1 & (T-\alpha)\\ 0 & 1\end{bmatrix} \tag{33}$$

Using symbolic tool in MATLAB, we can derive the closed-form expression of M_{pd} as follows:

$$M_{pd} = \begin{bmatrix}M_{11}M_{12}\\ M_{21}M_{22}\end{bmatrix}$$

where

$$M_{11} = \frac{C\,\mathrm{e}^{a\sqrt{C^2-2K}-Ca} - C\,\mathrm{e}^{-Ca-a\sqrt{C^2-2K}} + \mathrm{e}^{a\sqrt{C^2-2K}-Ca}\sqrt{C^2-2K} + \mathrm{e}^{-Ca-a\sqrt{C^2-2K}}\sqrt{C^2-2K}}{2\sqrt{C^2-2K}}$$

$$M_{12} = \frac{\mathrm{e}^{a\sqrt{C^2-2K}-Ca} - \mathrm{e}^{-Ca-a\sqrt{C^2-2K}}}{2\sqrt{C^2-2K}} + \frac{(T-a)\left(C\,\mathrm{e}^{a\sqrt{C^2-2K}-Ca} - C\,\mathrm{e}^{-Ca-a\sqrt{C^2-2K}} + \mathrm{e}^{a\sqrt{C^2-2K}-Ca}\sqrt{C^2-2K} + \mathrm{e}^{-Ca-a\sqrt{C^2-2K}}\sqrt{C^2-2K}\right)}{2\sqrt{C^2-2K}}$$

$$M_{21} = -\frac{K\,\mathrm{e}^{a\sqrt{C^2-2K}-Ca} - K\,\mathrm{e}^{-Ca-a\sqrt{C^2-2K}}}{\sqrt{C^2-2K}}$$

$$M_{22} = \frac{C\,\mathrm{e}^{-Ca-a\sqrt{C^2-2K}} - C\,\mathrm{e}^{a\sqrt{C^2-2K}-Ca} + \mathrm{e}^{a\sqrt{C^2-2K}-Ca}\sqrt{C^2-2K} + \mathrm{e}^{-Ca-a\sqrt{C^2-2K}}\sqrt{C^2-2K}}{2\sqrt{C^2-2K}} - \frac{(T-a)\left(K\,\mathrm{e}^{a\sqrt{C^2-2K}-Ca} - K\,\mathrm{e}^{-Ca-a\sqrt{C^2-2K}}\right)}{\sqrt{C^2-2K}}$$

2.3.3 General Solution of Poincare Map of Hybrid Linear Systems

$$\dot{Z} = AZ + B \tag{34}$$

where **A is invertible**. If the **mode transistion is time-based**, then we can augment the state of the system with t:

$$\dot{X} = \begin{bmatrix} \dot{t} \\ \dot{Z} \end{bmatrix} = \begin{bmatrix} 0 & 0 \\ 0 & A \end{bmatrix} X + \begin{bmatrix} 1 \\ B \end{bmatrix} \tag{35}$$

where $X = [t, Z]^T$. Assuming the mode trasition happened under the following condition:

$$e^T X = 0 \tag{36}$$

and takes time Δt from X_n to X_{n+1}, then the Poincare map (Jacobian matrix) can be expressed as:

$$\frac{\partial X_{n+1}}{\partial X_n} = -\dot{X}_{n+1}(e^T \dot{X}_{n+1})^{-1} e^T \begin{bmatrix} 1 & 0 \\ 0 & e^{A\Delta t} \end{bmatrix} + \begin{bmatrix} 1 & 0 \\ 0 & e^{A\Delta t} \end{bmatrix} \tag{37}$$

3 2D Spoked Runners

Extended from the vertical hopper, this model is aimed to use for analysis of coupled dynamics of the spoked runner, which has following assumptions

- massless leg

3.1 SLIP model with a locked flywheel

Compared to [43], this is a model which is genearlized so that the rotation in the flight phase can also be considered.

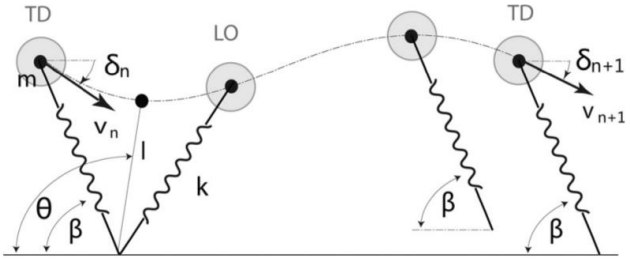

Fig. 1 The SLIP model. The parameters *m*, *k*, and *β* stand for body mass, leg stiffness, and landing angle, respectively. The CoM position during stance is characterized by leg length *l* and leg angle *θ*. Here, TD and LO stand for touchdown and liftoff, respectively.

Figure 3: The schematic of a SLIP model

3.1.1 System Kinematics

As indicated in Fig 3, the position of the body (mass) is

$$x = -lcos\theta$$
$$z = lsin\theta$$

and the velocity

$$\dot{x} = -\dot{l}cos\theta + lsin\theta\dot{\theta}$$
$$\dot{z} = \dot{l}sin\theta + lcos\theta\dot{\theta}$$

3.1.2 Lagrangian Mechanics

Wit the velocity of the mass, the Lagrangian L can be expressed as:

$$L = T - V = \frac{1}{2}m(\dot{x}^2 + \dot{y}^2) + \frac{1}{2}I\dot{\theta}^2 - V_{spring} - V_{gravity}$$
$$= \frac{1}{2}m(\dot{l}^2 + l^2\dot{\theta}^2) + \frac{1}{2}I\dot{\theta}^2 - \frac{1}{2}k(l - l_0)^2 - mg(lsin\theta)$$

where $I = mr_g^2$. Take l, θ as the generalized coordinate, the equation of motions are:
Stance Dynamics

$$m\ddot{l} - ml^2\dot{\theta}^2 + k(l - l_0) = -mgsin\theta$$
$$2m\dot{l}\dot{\theta} + m(l^2 + r_g^2)\ddot{\theta} + = -mglcos\theta$$

Flight Dynamics

$$\ddot{y} = -g$$
$$\ddot{\theta} = 0$$
$$\text{LO: } l = l_0$$
$$\text{TD: } y = l_0 sin\beta$$
$$(\text{Spoked TD: } \theta = \beta + \frac{2\pi}{d})$$

where β is the touch down angle, d is the number of the legs the spoked runner has.
Note: when $I = 0$, the system is equivalent to the transitional SLIP model as described in [43].

3.1.3 EOM of SLIP model with a locked fly wheel

This is an extended model which is used for the stability analysis of the 2D spoked (or reciprocating) runner.
Note: In the flight phase there will be the inertia at COM (the two masses connected via the link with length r_c), therefore no flywheel is required for the rotation EOM.

3.2 SLIP model with a pendulum

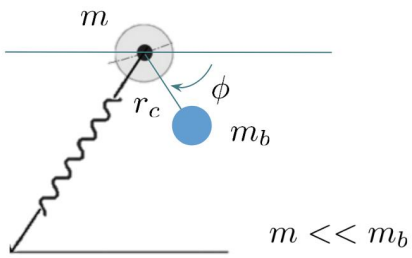

Figure 4: The schematic of a SLIP model

3.2.1 System Kinematics

As indicated in Fig 4, the position and the velocity of the frame m are:

$$x = -lcos\theta$$
$$z = lsin\theta$$
$$\dot{x} = -\dot{l}cos\theta + lsin\theta\dot{\theta}$$
$$\dot{z} = \dot{l}sin\theta + lcos\theta\dot{\theta}$$

The position and the velocity of the body m_b are:

$$x_b = -lcos\theta + r_c cos(\phi)$$
$$z_b = lsin\theta - r_c sin(\phi)$$
$$\dot{x}_b = -\dot{l}cos\theta + lsin\theta\dot{\theta} - r_c sin(\phi)(\dot{\phi})$$
$$\dot{z}_b = \dot{l}sin\theta + lcos\theta\dot{\theta} - r_c cos(\phi)(\dot{\phi})$$

3.2.2 Lagrangian Mechanics

Wit the velocity of the masses, the Lagrangian L can be expressed as:

$$\begin{aligned}
L =& T - V = \frac{1}{2}m(\dot{x}^2 + \dot{z}^2) + \frac{1}{2}m_b(\dot{x}_b^2 + \dot{z}_b^2) - V_{spring} - V_{gravity} - V_{b_{gravity}} \\
=& \frac{1}{2}m(\dot{l}^2 + l^2\dot{\theta}^2) + \frac{1}{2}m_b(\dot{l}^2 + l^2\dot{\theta}^2 + r_c^2\dot{\phi}^2 + 2\dot{\phi}r_c(\dot{l}sin(\phi-\theta) - l\dot{\theta}cos(\phi-\theta))) \\
& - \frac{1}{2}k(l-l_0)^2 - mg(lsin\theta) - m_bg(lsin\theta - r_csin\phi)
\end{aligned}$$

EOM of l:

$$\begin{aligned}
\frac{\partial L}{\partial l} &= -(m+m_b)gsin\theta + (m+m_b)l\dot{\theta}^2 - k(l-l_0) - m_br_c\dot{\phi}\dot{\theta}cos(\phi-\theta) \\
\frac{\partial L}{\partial \dot{l}} &= (m+m_b)\dot{l} + m_br_c\dot{\phi}sin(\phi-\theta) \\
\frac{d\partial L}{dt\partial \dot{l}} &= (m+m_b)\ddot{l} + m_br_c\ddot{\phi}sin(\phi-\theta) + m_br_c\dot{\phi}cos(\phi-\theta)(\dot{\phi}-\dot{\theta})
\end{aligned}$$

EOM of θ:

$$\begin{aligned}
\frac{\partial L}{\partial \theta} &= -(m+m_b)glcos\theta + m_br_c\dot{\phi}(-\dot{l}cos(\phi-\theta) - l\dot{\theta}sin(\phi-\theta)) \\
\frac{\partial L}{\partial \dot{\theta}} &= (m+m_b)l^2\dot{\theta} - m_br_c\dot{\phi}lcos(\phi-\theta) \\
\frac{d\partial L}{dt\partial \dot{\theta}} &= (m+m_b)l^2\ddot{\theta} + 2(m+m_b)l\dot{l}\dot{\theta} \\
& \quad - m_br_c\ddot{\phi}cos(\phi-\theta) - m_br_c\dot{\phi}\dot{l}cos(\phi-\theta) + m_br_c\dot{\phi}lsin(\phi-\theta)(\dot{\phi}-\dot{\theta})
\end{aligned}$$

EOM of ϕ:

$$\begin{aligned}
\frac{\partial L}{\partial \phi} &= m_bgr_ccos(\phi) + m_br_c\dot{\phi}(\dot{l}cos(\phi-\theta) + l\dot{\theta}sin(\phi-\theta)) \\
\frac{\partial L}{\partial \dot{\phi}} &= m_br_c^2(\dot{\phi}) + m_br_c(\dot{l}sin(\phi-\theta) - l\dot{\theta}cos(\phi-\theta)) \\
\frac{d\partial L}{dt\partial \dot{\phi}} &= m_br_c^2(\ddot{\phi}) + m_br_c(\ddot{l}sin(\phi-\theta) + \dot{l}cos(\phi-\theta)(\dot{\phi}-\dot{\theta})) \\
& \quad - m_br_c(\dot{l}\dot{\theta}cos(\phi-\theta) + l\ddot{\theta}cos(\phi-\theta) - l\dot{\theta}sin(\phi-\theta)(\dot{\phi}-\dot{\theta}))
\end{aligned}$$

Take l, θ, ϕ as the generalized coordinate, the equation of motions are:

$$\begin{aligned}
&(m+m_b)\ddot{l} + m_br_c\ddot{\phi}sin(\phi-\theta) + m_br_c\dot{\phi}cos(\phi-\theta)(\dot{\phi}-\dot{\theta}) = \\
&-(m+m_b)gsin\theta + (m+m_b)l\dot{\theta}^2 - k(l-l_0) - m_br_c\dot{\phi}\dot{\theta}cos(\phi-\theta) \\
&(m+m_b)l^2\ddot{\theta} + 2(m+m_b)l\dot{l}\dot{\theta} - m_br_c\ddot{\phi}cos(\phi-\theta) - m_br_c\dot{\phi}\dot{l}cos(\phi-\theta) + m_br_c\dot{\phi}lsin(\phi-\theta)(\dot{\phi}-\dot{\theta}) = \\
&-(m+m_b)glcos\theta + m_br_c\dot{\phi}(-\dot{l}cos(\phi-\theta) - l\dot{\theta}sin(\phi-\theta)) \\
&m_br_c^2(\ddot{\phi}) + m_br_c(\ddot{l}sin(\phi-\theta) + \dot{l}cos(\phi-\theta)(\dot{\phi}-\dot{\theta})) - m_br_c(\dot{l}\dot{\theta}cos(\phi-\theta) + l\ddot{\theta}cos(\phi-\theta) - l\dot{\theta}sin(\phi-\theta)(\dot{\phi}-\dot{\theta})) = \\
&m_bgr_ccos(\phi) + m_br_c\dot{\phi}(\dot{l}cos(\phi-\theta) + l\dot{\theta}sin(\phi-\theta))
\end{aligned}$$

Rearrange the EOMs and move all terms without accelerations to the right hand side:

$$
\begin{aligned}
&\ddot{l}(m+m_b) + \ddot{\phi} m_b r_c sin(\phi-\theta) = \\
&-m_b r_c \dot{\phi} cos(\phi-\theta)(\dot{\phi}-\dot{\theta}) - (m+m_b) g sin\theta + (m+m_b) l\dot{\theta}^2 - k(l-l_0) - m_b r_c \dot{\phi}\dot{\theta} cos(\phi-\theta) \\
&\ddot{\theta}(m+m_b) l^2 - \ddot{\phi} m_b r_c cos(\phi-\theta) = \\
&-2(m+m_b) l\dot{l}\dot{\theta} + m_b r_c \dot{\phi}\dot{l} cos(\phi-\theta) - m_b r_c \dot{\phi} l sin(\phi-\theta)(\dot{\phi}-\dot{\theta}) - (m+m_b) g l cos\theta + m_b r_c \dot{\phi}(-\dot{l} cos(\phi-\theta) - l\dot{\theta} sin(\phi-\theta)) \\
&\ddot{\phi} m_b r_c^2 + \ddot{l} m_b r_c sin(\phi-\theta) - \ddot{\theta} m_b r_c l cos(\phi-\theta) = \\
&-m_b r_c \dot{l} cos(\phi-\theta)(\dot{\phi}-\dot{\theta}) + m_b r_c (\dot{l}\dot{\theta} cos(\phi-\theta) - l\dot{\theta} sin(\phi-\theta)(\dot{\phi}-\dot{\theta})) \\
&+ m_b g r_c cos(\phi) + m_b r_c \dot{\phi}(\dot{l} cos(\phi-\theta) + l\dot{\theta} sin(\phi-\theta))
\end{aligned}
$$

Equation of motion of the stance phase in matrix form:

$$
\begin{aligned}
\ddot{X} &= \begin{bmatrix} \ddot{l} \\ \ddot{\theta} \\ \ddot{\phi} \end{bmatrix} \\
&= M^{-1} \begin{bmatrix} -m r_c \dot{\phi} cos(\phi-\theta)(\dot{\phi}-\dot{\theta}) - (m_f+m) g sin\theta + (m_f+m) l\dot{\theta}^2 - k(l-l_0) - m r_c \dot{\phi}\dot{\theta} cos(\phi-\theta) \\ -2(m_f+m) l\dot{l}\dot{\theta} + m r_c \dot{\phi}\dot{l} cos(\phi-\theta) - m r_c \dot{\phi} l sin(\phi-\theta)(\dot{\phi}-\dot{\theta}) - (m_f+m) g l cos\theta + m r_c \dot{\phi}(-\dot{l} cos(\phi-\theta) - l\dot{\theta} sin(\phi-\theta)) \\ -m r_c \dot{l} cos(\phi-\theta)(\dot{\phi}-\dot{\theta}) + m r_c (\dot{l}\dot{\theta} cos(\phi-\theta) - l\dot{\theta} sin(\phi-\theta)(\dot{\phi}-\dot{\theta})) + m g r_c cos(\phi) + m r_c \dot{\phi}(\dot{l} cos(\phi-\theta) + l\dot{\theta} sin(\phi-\theta)) \end{bmatrix} \quad (1)
\end{aligned}
$$

$$
\text{LO: } l = l_0 \quad (2)
$$

where M is the inertia matrix:

$$
M = \begin{bmatrix} m+m_f & 0 & m r_c sin(\phi-\theta) \\ 0 & (m+m_f) l^2 & -m r_c cos(\phi-\theta) \\ m r_c sin(\phi-\theta) & -m r_c cos(\phi-\theta) & m r_c^2 \end{bmatrix} \quad (3)
$$

Equation of motion in flight phase

$$
\ddot{x}_c = -g \quad (4)
$$

$$
\ddot{\phi} = 0 \quad (5)
$$

$$
\text{TD: } y_c + \frac{m}{m+m_f} r_c sin(\phi) = l_0 sin(\beta) \quad (6)
$$

where z_c is the center of mass vertical position. With the initial positions and velocities of the point mass m and m_f, the initial condition $[z_c, \dot{z}_c, \phi, \dot{\phi}]^T$ of the flight phase can be determined via linear and angular momentum conservation.

Dimension analysis:

- Mass is scaled by m: $\tilde{m} = 1$, $\tilde{m}_f = m_f/m$
- Length is scaled by l_0: $\tilde{l} = l/l_0$,$\tilde{r}_c = r_c/l_0$
- Time is scaled by $l_0/v_0 \rightarrow \tilde{g} = g l_0/v_0$, $\tilde{k} = k l_0^2/m v_0^2$

4 Simulations

4.1 Abstract Runner with Open-loop Normal Force and Closed-loop Pitch Angle Control

System Setup

- Body mass $m = 10$, $I_{yy} = 10$ with massless leg, $l = 1$.
- Reuse the vertical hopper above, change the initial condition to $\theta = 0.2$
- No force applied in the x direction, $\dot{x}_0$ can be 0 (hopper) or a constant (runner).
- Similar to the abstract runner (Fig. 5), enforces the on/off timing of ground reaction force $f_n(t)$:

$$f_n(t) = \begin{cases} (f_n + u) | f_n \in \mathbb{C}, & \text{if } t \in t_{on}. \\ 0, & \text{otherwise.} \end{cases}$$

where $f_n = \alpha * mg$, $\alpha \in \mathbb{C}$, u is the force from PD control, $kp_z = 80, kd_z = 6$. $kp_{pitch} = 80, kd_{pitch} = 6$

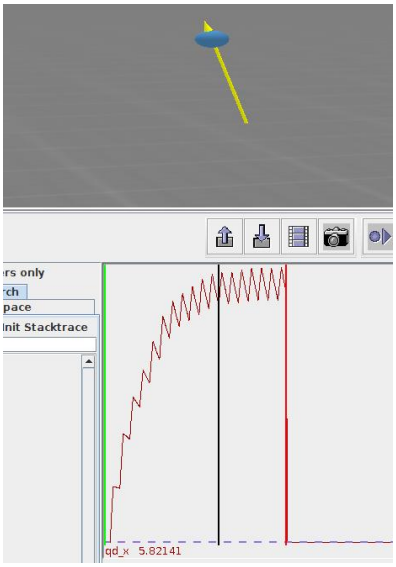

Figure 5: The Abstract Runner

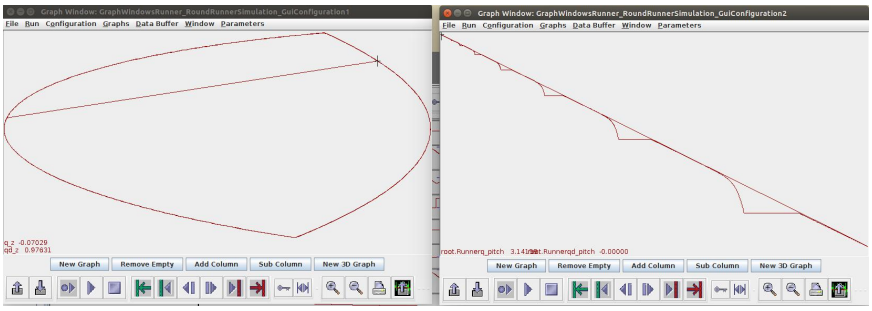

Figure 6: The phase portrait of the abstract runner: phase portrait (left) of body z movement $[q\_z, qd\_z]^T$ and the pitch motion (right, the movement is converging to the origin in the upper-left corner) .

Plan

- Link it to the Math from Jerry's note (analysis of a linear Poincare map) to get the boundaries of stable parameters.

4.2 Spoked Runner with Massless Legs

System Setup

- $m = 15$, $I_{yy} = 10$, $l = 4$, $r_{penetration} = 0.3$ (the distance the virtual wheel penetrate into the ground)
- Adjustable spoke leg number
- Fixed rotation rate w.r.t inertial frame
- Setup of contact force: PD control
  - w.r.t to world frame
  - w.r.t to inertial frame (virtual pivot point)
- Assuming no friction (Could be an bad idea?)

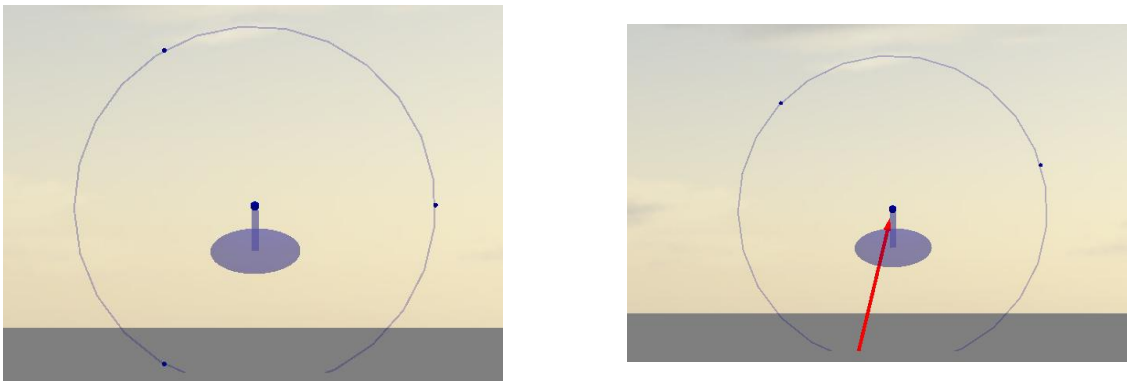

Figure 7: The Spoked Runner with three legs

Plan

- Smoothly change the leg length, or the rotational speed of the virtual wheel, and observe the system response.
- Learn how to use GUI for parameter adjustment with SCS.

5 Code implementation

5.1 Modeling and Parameters

Main idea: a virtual wheel (as the massless leg) with radius r_{wheel} penetrate the ground for a distance r_{pen} where a external force point pe is attached on it. A body (with mass m and inertia Iyy) is attached to the center of wheel. Using PD control to interpret contact force when p_e is under the ground.

06/07 First prototype (Not used now)

- Joint numbers: 2
- Joint types: Floating planer joint for virtual wheel and pin joint for the body link.
- Contact point type: External force point
- Virtual wheel rotation: set proper initial condition for virtual wheel (also need a large inertia to make it nearly constant).

Contact force: Assuming the ground height is 0,

$$F_z = kp(0 - pe_z) + kd(0 - ve_z) \tag{1}$$
$$\phi = atan2(pe_x, r_{wheel} - pe_z) \tag{2}$$
$$F_x = F_z tan(\phi) \tag{3}$$

where ve is the velocity vector of the contact point pe, kp and kd are the PD control parameters. F_x is calculated so that the vector of ground reaction force $[F_x, F_y, F_z]^T$ will point towards the virtual pivot (the center of the virtual wheel).

Assessments:

- Need to set a non-zero inertia of massless virtual wheel (for numerical stability), otherwise the simulation will diverge.
- The inertia of virtual wheel need to be a large one for constant rotational speed.
- Suggestions: remove the massless link, attach the external force point to the body and change its position in the controller every time step.

06/08 Round Runner

- Joint numbers: 1
- Joint types: Floating planer joint for the body link.
- Contact point type: External force point
- Virtual wheel rotation: Assigning the external force point location with respect to the joint in an open loop manner.
- Contact force: Assuming the ground height is 0,

$$F_z = kp(0 - pe_z) + kd(0 - ve_z) \tag{4}$$
$$\phi = atan2(pe_x, r_{wheel} - pe_z) \tag{5}$$
$$F_x = F_z tan(\phi) \tag{6}$$

where ve is the velocity vector of the contact point pe, kp and kd are the PD control parameters. F_x is calculated so that the vector of ground reaction force $[F_x, F_y, F_z]^T$ will point towards the virtual pivot (the center of the virtual wheel).

Assessments:

- The ground reaction force looks better, while the energy is not balanced (after a while it will move towards the negative x direction)
- The inertia of virtual wheel need to be a large one for constant rotational speed.
- Suggestions: Use the ground contact point (instead of external force point) to see how it goes.

06/11 Round Runner(with Ground Contact Point)

- Joint numbers: 1
- Joint types: Floating planer joint for the body link.
- Contact point type: Ground contact point, linear contact model[1]
- Virtual wheel rotation: Assigning the external force point location with respect to the joint in an open loop manner.
- **Contact point number** Parameterized, currently set to 3-6 points.
- Contact force: using built-in functionalities, only assigning the kp, kd (PD parameters in the z direction), kp_x, and kd_x (PD parameters in the x/y directions).

Assessments:

- Was able to generate a stable walking. Contact point has sliding.
- Due to setting up stiffness and damping for x and z separately, the force is not always point towards the virtual pivot.

06/12 Round Runner(with External Contact Point Point)

- Implement the same one as 06/11, but replace the ground contact point to the external one (because it is more complex for ground contact point to adjust stiffness/damping as parameters.)
- implement the linear ground contact model basically.

06/13 Round Runner

- Parameterize contact point numbers
- Adding enum for switching between different setup: contact point type and the corresponding ground reaction force calculation: (w.r.t to the world frame or inertia frame.)

06/16 Round Runner (vertical hopper)

- Adding vertical hopper with open-loop force control
- Playing with open-loop force magnitudes for different stability conditions

[1]Disable the hardening stiffness in z direction by setting groundStiffeningLength to Double.NEGATIVE_INFINITY

6 Info might be useful

6.1 Finding a fixed-point solution from numerical Poincare map

If the analytical solution of Poincare map can be derived, then one can obtain the fixed-point easily. The followings are related methods (best to my knowledge) to get fixed-points of Poincare map through simulations:

Finding stable fixed-points
Take a collection of state at Poincare section defined (e.g. at touch down, or the end of the support phase, etc.) as $[x_1, x_2, \ldots, x_n]'$. Take the first $n-1$ states as $X_n = [x_1, x_2, \ldots, x_{n-1}]'$ and the last $n-1$ states as $X_{n+1} = [x_2, x_3, \ldots, x_n]'$, the map A can be approximated as:

$$\begin{aligned} X_{n+1} &= A(X_n) \\ \rightarrow A &= X_{n+1}/(X_n) \end{aligned}$$

If the system as a stable fixed point x^*, then the following should be satisfied:

$$\lim_{n\to\infty} x^* = x_n = Ax_{n-1} = A^n x_1 = x_{n-1}$$

Note:

- If A is invertible, the unstable fixed point might be derived it by calculating the Poincare section in the backward manner.
- Whether the fixed-point is accurate enough is also depending on the quality of data (whether the data is sufficiently rich).
- Unlike the method like PCA, the data can only being subtracted by the fixed-point, otherwise the dynamics will be changed (scaling like dimensionless analysis is okay).

Finding fixed-points
The more general way to find fixed-point is to simulate the system, and evaluate the difference of the periodic condition at the Poincare section as the cost/constraint. Trajectory Optimization

- Single Shooting
- Multiple Shooting
- Direct Collocation

6.2 Going through references

1. Compare different terrestiral locomotions: Some parameters of the walk are not speed- dependent. The swing duration is a constant time parameter [1].
2. Trunk plays an important role during walking (birds) [2].
3. The use of these drives (Resonance drives, with adaptive control) allows increasing machine's quickness several times and decreasing energy expenses simultaneously 10-50 times [3].
4. Light weight leg (ostrich vs. moa) can run faster[5]. Also a famous allometric equation:

   $$Y = M^{3/4} \tag{1}$$

   where M is the body mass, Y is the metabolic rate.
5. Human's walking may not be really self-optimized: the preferred speed maybe different from the energetically optimal speed[8].

6. It is concluded that the most important adjustment to the body's spring system to accommodate higher stride frequencies is that leg spring becomes stiffer [19].

7. magic equations for imd force (ostrich) [26]

8. gait frequency was reported to be highly correlated with the resonant frequency of the mass-spring model [30]

9. WABIAN, why you are here? [31]

6.3 Categories

1. Nonlinear oscillators/components [3, 6, 9, 10, 12, 28, 39];

2. zoology, biomechanics of animals: [1, 2, 4, 5, 16]

3. Bio-inspired robots: [7, 32]

4. Reference I should read: [11, 15, 27, 28]

5. Article not found (or not free)[4].

6. Robots in 3D: [13]

7. Stability analysis (Monocycle, linearized system) [14] (Limit cycle) [11, 27] dimensionless [42]

8. Biology/Anatomical structure [17, 20]

9. Light weight fast robot [18, 25]

10. take a look again [21]

11. mechanism design of robot [22]

12. quadruped reference [23] MIT Cheetah[37]

13. human energy cost, resonance usage [24, 8, 38, 40]

14. walking parameterization [29, 21, 44]

15. human-animal differences [15]

16. open-loop robot [33], passive robot [35, 34, 36]

References

[1] Anick Abourachid. Kinematic parameters of terrestrial locomotion in cursorial (ratites), swimming (ducks), and striding birds (quail and guinea fowl). *Comparative Biochemistry and Physiology Part A: Molecular and Integrative Physiology*, 131(1):113–119, dec 2001.

[2] Anick Abourachid, Remi Hackert, Marc Herbin, Paul A. Libourel, François Lambert, Henri Gioanni, Pauline Provini, Pierre Blazevic, and Vincent Hugel. Bird terrestrial locomotion as revealed by 3D kinematics. *Zoology*, 114(6):360–368, dec 2011.

[3] T. Akinfiev and M. Armada. Elements of built-in diagnostics for resonance drive with adaptive control system. In *International Symposium on Automation and Robotics in Construction*, pages 617–621, Madrid, Spain, 1999.

[4] R. Mc N Alexander, G. M O Maloiy, R. Njau, and A. S. Jayes. Mechanics of running of the ostrich (Struthio camelus). *Journal of Zoology*, 187(2):169–178, 1979.

[5] R. McNeill Alexander. The legs of ostriches (Struthio) and moas (Pachyornis). *Acta Biotheoretica*, 34(2-4):165–174, 1985.

[6] G. V. Anand. Nonlinear Resonance in Stretched Strings with Viscous Damping. *The Journal of the Acoustical Society of America*, 40(6):1517–1528, 1966.

[7] Arvind Ananthanarayanan, Mojtaba Azadi, and Sangbae Kim. Towards a bio-inspired leg design for high-speed running. *Bioinspiration and Biomimetics*, 7(4):046005, dec 2012.

[8] Elizabeth Arnall, Jessica Pyatt, Chelsie Rice, Katie L Anderson, and Duncan Mitchell. Resonance in Human Walking Economy: How Natural Is It? *International Journal of Undergraduate Research and Creative Activities*, 4(1), 2012.

[9] V. I. Babitsky and M. Y. Chitayev. Adaptive high-speed resonant robot. *Mechatronics*, 6(8):897–913, dec 1996.

[10] Jonas Buchli, Fumiya Iida, and Auke Jan Ijspeert. Finding resonance: Adaptive frequency oscillators for dynamic legged locomotion. In *IEEE International Conference on Intelligent Robots and Systems*, pages 3903–3909, Beijing, China, 2006.

[11] J. G. Cham. *On Performance and Stability in Open-Loop Running*. PhD thesis, Stanford University, 2002.

[12] S. Chatterjee and Anindya Malas. On the stiffness-switching methods for generating self-excited oscillations in simple mechanical systems. *Journal of Sound and Vibration*, 331(8):1742–1748, apr 2012.

[13] Michael J. Coleman, Anindya Chatterjee, and Andy Ruina. Motions of a rimless spoked wheel: a simple three-dimensional system with impacts. *Dynamics and Stability of Systems*, 12(3):139–159, 1997.

[14] Michael J. Coleman and Jim M. Papadopoulos. Intrinsic stability of a classical monocycle and a generalized monocycle. In *Bicycle and Motorcycle Dynamics, Symposium on Dynamics and Control of Single Track Vehicles*, Delft, Netherlands, 2010.

[15] M. A. Daley and A. A. Biewener. Running over rough terrain reveals limb control for intrinsic stability. *Proceedings of the National Academy of Sciences*, 103(42):15681–15686, oct 2006.

[16] M. A. Daley, G. Felix, and A. A. Biewener. Running stability is enhanced by a proximo-distal gradient in joint neuromechanical control. *Journal of Experimental Biology*, 210(3):383–394, feb 2007.

[17] T. El-Mahdy, S. M. El-Nahla, L. C. Abbott, and S. A.M. Hassan. Innervation of the pelvic limb of the adult ostrich (Struthio camelus). *Journal of Veterinary Medicine Series C: Anatomia Histologia Embryologia*, 39(5):411–425, 2010.

[18] Darrell Ethington. Dash Robotics Reveals A DIY High-Speed Running Robot Kit, Which Hobbyists Can Own For Just $65, 2013.

[19] Claire T. Farley and Octavio González. Leg stiffness and stride frequency in human running. *Journal of Biomechanics*, 29(2):181–186, 1996.

[20] D. Gangl, G. E. Weissengruber, M. Egerbacher, and G. Forstenpointner. Anatomical description of the muscles of the pelvic limb in the ostrich (Struthio camelus). *Journal of Veterinary Medicine Series C: Anatomia Histologia Embryologia*, 33(2):100–114, 2004.

[21] S. M. Gatesy and A. A. Biewener. Bipedal locomotion: effects of speed, size and limb posture in birds and humans. *Journal of Zoology*, 224(1):127–147, 1991.

[22] Martin Grimmer and André Seyfarth. Design of a Series Elastic Actuator driven ankle prosthesis : The trade-off between energy and peak power optimization. In *Dynamic Walking*, 2011.

[23] R Hackert, H Witte, and M S Fischer. Interactions between motions of the trunk and the angle of attack of the forelimbs in synchronous gaits of the pika (Ochotona rufescens). In *Adaptive Motion of Animals and Machines*, pages 69–77. Springer, 2006.

[24] Kenneth G. Holt, Joseph Hamill, and Robert O. Andres. Predicting the minimal energy costs of human walking. *Medicine & Science in Sports & Exercise*, 23(4):491–498, 1991.

[25] Fumiya Iida, Murat Reis, Nandan Maheshwari, Xiaoxiang Yu, and Amir Jafari. Toward efficient, fast, and versatile running robots based on free vibration. In *Dynamic Walking*, Pensacola, FL, 2012.

[26] D. L. Jindrich, N. C. Smith, K. Jespers, and A. M. Wilson. Mechanics of cutting maneuvers by ostriches (Struthio camelus). *Journal of Experimental Biology*, 210(8):1378–1390, 2007.

[27] Takahiro Kagawa and Yoji Uno. Necessary condition for forward progression in ballistic walking. *Human Movement Science*, 29(6):964–976, dec 2010.

[28] Jg Daniël Karssen and Martijn Wisse. Running with improved disturbance rejection by using non-linear leg springs. *International Journal of Robotics Research*, 30(13):1585–1595, sep 2011.

[29] Leng Feng Lee and Venkat N. Krovi. Musculoskeletal simulation-based parametric study of optimal gait frequency in biped locomotion. In *International Conference on Biomedical Robotics and Biomechatronics*, pages 354–359, Scottsdale, AZ, 2008.

[30] Myunghyun Lee, Seyoung Kim, and Sukyung Park. Leg stiffness increases with load to achieve resonance-based CoM oscillation. In *Dynamic Walking*, Pittsburgh, PA, 2013.

[31] Hun-ok Lim, Y Ogura, Atsuo Takanishi, and Proc R Soc A. Locomotion pattern generation and mechanisms of a new biped walking machine. *Proceedings of the Royal Society of London A: Mathematical and Physical Sciences*, 464(2089):273–288, 2008.

[32] R. J. Lock, S. C. Burgess, and R. Vaidyanathan. Multi-modal locomotion: From animal to application. *Bioinspiration and Biomimetics*, 9(1), dec 2014.

[33] Katja Mombaur, H Georg Bock, Johannes Schlöder, and Richard Longman. Stable Walking and Running Robots Without Feedback. In *Climbing and Walking Robots*, pages 725–735. 2005.

[34] Dai Owaki, Masatoshi Koyama, Shin'ichi Yamaguchi, Shota Kubo, and Akio Ishiguro. A two-dimensional passive dynamic running biped with knees. In *Proceedings - IEEE International Conference on Robotics and Automation*, pages 5237–5242, 2010.

[35] Dai Owaki, Masatoshi Koyama, Shin'Ichi Yamaguchi, Shota Kubo, and Akio Ishiguro. A 2-D passive-dynamic-running biped with elastic elements. *IEEE Transactions on Robotics*, 27(1):156–162, 2011.

[36] Dai Owaki, Koichi Osuka, and Akio Ishiguro. Understanding the common principle underlying passive dynamic walking and running. *2009 IEEE/RSJ International Conference on Intelligent Robots and Systems, IROS 2009*, pages 3208–3213, 2009.

[37] Hae-won Park, Sangbae Kim, and Our Approach. Variable Speed Galloping Control using Vertical Impulse Modulation for Quadruped Robots : Application to MIT Cheetah Robot Click for Video Overview, 2012.

[38] Sukyung Park. Can human walking be mimicked by resonance-based oscillation? In *The 7th World Congress on Biomimetics, Artificial Muscles and Nano-Bio*, volume 44, page 2013, Jeju Island, South Korea, 2013.

[39] M C Plooij and M Wisse. A spring mechanism for resonant robotic arms. In *Workshop on Human Friendly Robotics*, page 5, 2011.

[40] V. Racic, A. Pavic, and J. M.W. Brownjohn. Experimental identification and analytical modelling of human walking forces: Literature review. *Journal of Sound and Vibration*, 326(1-2):1–49, sep 2009.

[41] C. David Remy. *Optimal exploitation of natural dynamics in legged locomotion.* PhD thesis, ETH Zurich, July 2011.

[42] Sebastian Riese and Andre Seyfarth. Stance leg control: Variation of leg parameters supports stable hopping. *Bioinspiration and Biomimetics*, 7(1):016006, mar 2012.

[43] Zhuohua Shen and Justin Seipel. A Piecewise-Linear Approximation of the Canonical Spring-Loaded Inverted Pendulum Model of Legged Locomotion. *Journal of Computational and Nonlinear Dynamics*, 11(1):011007, 2016.

[44] Robert E Weems. Locomotor Speeds and Patterns of Running Behavior in Non-Maniraptoriform Theropod Dinosaurs. *New Mexico Museum of Natural History and Science Bulletin*, 37:379–389, 2006.